

High-resolution FTIR spectroscopy and analysis of the $K_a = 0 \leftarrow 1$ subbands of the fundamentals ν_3 and ν_6 of the dimer $(\text{HF})_2$

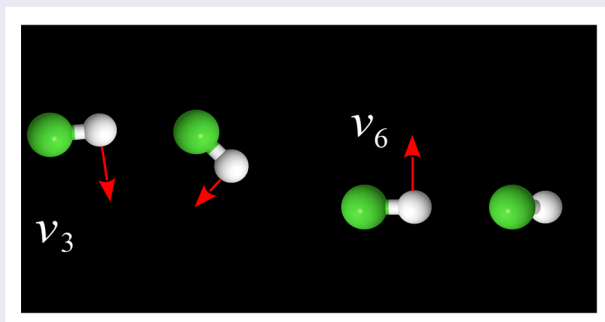
H. Hollenstein^{a*}, M. Hippler^{a,b}, G. Seyfang^a and M. Quack^a

^aDepartment of Chemistry and Applied Biosciences, ETH Zürich, Zürich, Switzerland; ^bDepartment of Chemistry, University of Sheffield, Sheffield, England

ABSTRACT

We report new far-infrared spectra of $(\text{HF})_2$ obtained by high resolution long-path Fourier Transform-Infrared (FTIR) spectroscopy. The origins of the two tunneling components of the $K_a = 0 \leftarrow 1$ subband of the in-plane symmetric bending fundamental ν_3 were found to be at 450.4546 cm^{-1} ($\Gamma_t: A^+ \leftarrow B^+$) and at 451.4583 cm^{-1} ($B^+ \leftarrow A^+$), and of the $K_a = 0 \leftarrow 1$ subband of the out-of-plane bending fundamental ν_6 at 382.0802 cm^{-1} ($A^+ \leftarrow A^+$) and at 383.2245 cm^{-1} ($B^+ \leftarrow B^+$). The $K_a = 0$ term values with respect to the ground state $\Gamma_t = A^+$ term are 486.9442 cm^{-1} for the A^+ and 486.8834 cm^{-1} for the B^+ tunneling levels of ν_3 . They are 417.5053 cm^{-1} for the A^- and 419.7140 cm^{-1} for the B^- vibration-tunneling sublevels of ν_6 . The results are discussed in relation to full-dimensional quantum dynamics and predictions based on recent *ab initio* calculations and our empirically refined potential energy hypersurfaces.

Graphical abstract



ARTICLE HISTORY

Received 8 March 2024

Accepted 4 April 2024

KEYWORDS






FTIR spectroscopy; HF dimer; potential energy hypersurfaces; vibration-tunneling dynamics; hydrogen bonding

1. Introduction

In contrast to early theoretical analyses of high-resolution spectra of polyatomic molecules and clusters based on perturbation theory and approximate vibration rotation Hamiltonians, recent progress has focused on quasi-exact vibration rotation calculations on full-dimensional potential hypersurfaces (see for instance the reviews in [1]). Attila Császár has been a pioneer in the development of exact numerical methods and computational approaches towards such molecular rovibrational eigenstate calculations [2,3]. In particular the highly non-rigid hydrogen bonded clusters are candidates for such

approaches and an early example for vibration-tunneling quantum dynamics on full-dimensional potential hypersurfaces is the prototypical dimer HFHF [4]. Some of the historical development can be found summarized in the recent Refs. [5,6].

Indeed, the hydrogen bonded clusters $(\text{HF})_n$ can be considered to be the simplest prototypes for studies of multidimensional potential hypersurfaces and the quantum dynamics of hydrogen bond tunneling rearrangement and hydrogen bond formation and dissociation processes in hydrogen-bonded clusters in general [7–9]. Such clusters in increasing size (with $n = 2, 3, 4, \dots$,

CONTACT M. Hippler  M.Hippler@sheffield.ac.uk  Department of Chemistry and Applied Biosciences, ETH Zürich, CH-8093 Zürich, Switzerland; Department of Chemistry, University of Sheffield, S3 7HF Sheffield, England,  <https://michaelhippler.sites.sheffield.ac.uk>; M. Quack  Martin@Quack.ch Department of Chemistry and Applied Biosciences, ETH Zürich, CH-8093 Zürich, Switzerland,  www.ir.ethz.ch

*Dr. sc. nat. Hans Hollenstein, 27/2/1941–5/5/2023

© 2024 The Author(s). Published by Informa UK Limited, trading as Taylor & Francis Group.

This is an Open Access article distributed under the terms of the Creative Commons Attribution License (<http://creativecommons.org/licenses/by/4.0/>), which permits unrestricted use, distribution, and reproduction in any medium, provided the original work is properly cited. The terms on which this article has been published allow the posting of the Accepted Manuscript in a repository by the author(s) or with their consent.

up to very large nanoclusters [10–14]) can serve as a role model for the transition from molecules in the gas phase to liquids and solids also for more complex hydrogen-bonded systems such as water, alcohols and even biomolecular systems such as proteins and DNA [15–21]. They can also serve in relation to effects such as quasiadiabatic channel above barrier tunneling to an understanding of some of the most fundamental aspects of tunneling spectra [5,22].

Although the hydrogen bond in the HF dimer is relatively strong, with electronic dissociation energy corresponding to $D_e = 1597 \text{ cm}^{-1}$ by theory [4,7,23] and $D_0 = 1062 \text{ cm}^{-1}$ ($\Delta H_0^\ominus = 12.70 \text{ kJ mol}^{-1}$) by experiment [24,25], this molecule is very flexible and the description of its dynamics is quite complicated. Considering its degrees of freedom, we may distinguish between the so-called intramolecular vibrations ν_1 (*free* HF stretching) and ν_2 (*bonded* HF stretching), and the intermolecular modes ν_3 (in-plane symmetric bending or in-plane libration or ‘antigear’ bend or conrotatory bend), ν_4 (FF stretch or van der Waals stretch), ν_5 (in-plane antisymmetric bend or ‘geared’ bend or hydrogen bond exchange disrotatory in-plane vibration) and ν_6 (out-of-plane bend or out-of-plane libration or out-of-plane torsion). The intermolecular fundamentals are expected below about 600 cm^{-1} , *i.e.* in the far infrared region. The far-infrared spectrum therefore represents a particularly rich source of information on structure and dynamics of this molecule. Early investigations of the far-infrared spectrum could identify the $K_a = 1 \leftarrow 0$ [26] and $2 \leftarrow 1$ [27] subbands of the ν_6 fundamental as well as excited K_a levels of the vibrational ground state ν_0 [27,28], ν_5 [29], and an approximate value of ν_4 [4]. Many structures in the far-infrared spectrum remained unexplained. In particular, the band centers ($K_a = 0$ levels) of the in-plane symmetric bending fundamental ν_3 and of the out-of-plane bending fundamental ν_6 were not experimentally assigned and analyzed in earlier work.

This lack of direct evidence motivated us to reinvestigate the far-infrared region of the spectrum by high resolution FTIR spectroscopy under improved conditions using a new long path absorption cell. We report the detailed analysis of two subbands centered near 380 and 450 cm^{-1} , which could be assigned to the $K_a = 0 \leftarrow 1$ subbands of the fundamentals ν_6 and ν_3 , respectively. The results of the present investigation are particularly timely in view of recent efforts of generating improved *ab initio* potential energy hypersurfaces [7,23,29–31]. The interaction potential of the two HF molecules in $(\text{HF})_2$ has been repeatedly studied already from the early days of accurate *ab initio* quantum chemistry [32–35]. A large set of *ab initio* potential energies for various structures calculated by Kofranek, Lischka and Karpfen [36] was

used as starting point for developing fully six dimensional analytical potential hypersurface representations by Quack and Suhm [4,37] (labeled QSKLK, QSBDE *etc.*, where the S in front indicates potentials which were semi-empirically adjusted to selected experimental data such as rotational constants B or the dissociation energy corresponding to D_e). These surfaces were used for full-dimensional eigenstate calculations by Quantum Monte Carlo techniques [4] as well as vibrational variational approaches [38,39]. In comparison with experiment it was noted that *ab initio* calculations needed improvement and a substantial effort led to new *ab initio* calculations using an MP2-R12 approach to generate accurate potential energy and dipole hypersurfaces [23,29]. At the same time, new high level CCSD(T) calculations were carried out for selected structures and properties [40,41]. It was realised that for some aspects of the empirical adjustment of the hypersurfaces the accurate spectroscopic basis was still lacking [4,23]. However, we have recently shown that the empirically adjusted potential hypersurface SO-3 from [7,29] provides a very satisfactory description of the HF-stretching overtone polyads including the tunneling and symmetry substructures [6,42]. Nevertheless, an accurate empirical basis for an adjustment notably for the properties related to the mode ν_3 is lacking and the present work intends to fill this gap.

2. Experimental

The high-resolution spectra have been measured on our BOMEM DA002 spectrometer in the $125\text{--}680 \text{ cm}^{-1}$ range (see Refs. [26–28,43,44]). We used a Globar light source, a 3μ Mylar beam splitter and a liquid Helium cooled Si bolometer which was equipped with a $12.5 \mu\text{m}$ cut-on long wave pass filter. The sample cell had been purchased from *Portmann Instruments AG, Switzerland*. It is a coolable long-path cell with internal White optics. The base length is 1.37 m and the path length can be varied in steps of about 10 m . The cooling of the cell can be performed by passing a refrigerant through a cooling-jacket. All materials of the cell have been carefully selected to be resistant to HF. The cell body is made of stainless steel and the White optics inside the cell consists of gold coated CaF_2 mirrors. The cell was equipped with polyethylene windows and was cooled to 243 K by passing cryogenic liquid from a thermostat (Lauda Kryomat RUK90, Instrumentengesellschaft AG, Zürich). The optical path length was set to 30 m and the HF pressure was chosen in the $15\text{--}20 \text{ mbar}$ range. Under these conditions the spectra taken at a resolution of 0.01 cm^{-1} are limited by pressure broadening. In order to improve the signal-to-noise ratio, we co-added 100

scans in a typical measurement. The wavenumber calibration was done with *in situ* H₂O lines (see [44–46]). The estimated wavenumber uncertainty, given by the root-mean-square (rms) deviation of 57 calibration lines in the range 200–530 cm⁻¹ with respect to a linear calibration function, was $d_{\text{rms}} = 1.2 \times 10^{-3} \text{ cm}^{-1}$.

3. Term formulae and selection rules

The dimer (HF-HF) is a slightly bent, near symmetric top. As it is fairly flexible, each sublevel of a given symmetric top quantum number K ($= K_a$) is best characterised by an individual set of spectroscopic parameters [26]. For the rotational analysis of vibration-tunneling K -subbands involving K_a up to 2 the following term formula (1) proved successful in previous studies [26,27,28,43,47] and will be used in the present analyses (see in particular [47] also for the symmetry selection rules):

$$\begin{aligned} \frac{E_{vK}^{(\pm)}}{hc} = & \tilde{\nu}_{vK} + \left(\bar{B}_{vK} \pm \frac{1}{4} \delta_{K1} b_{vK} \right) J(J+1) \\ & - [D_{vK} \mp (\delta_{K1} + \delta_{K2}) d_{vK}] J^2 (J+1)^2 \\ & + (H_{vK} \pm \delta_{K2} h_{vK}) J^3 (J+1)^3 \end{aligned} \quad (1)$$

The constant term $\tilde{\nu}_{vK}$ describes a hypothetical vibration-tunneling level for a fixed K , and J extrapolated to zero. $\bar{B}_{vK} = \frac{(B_{vK} + C_{vK})}{2}$ is an average rotational constant, D_{vK} and H_{vK} are centrifugal distortion constants, and $b_{vK} = (B_{vK} - C_{vK})$, d_{vK} and h_{vK} are asymmetry splitting constants of different order. The δ_{Ki} ($i = 1, 2$) are the conventional Kronecker delta. The upper signs in the above equation apply to levels with $K_a + K_c = J$, the lower to $K_a + K_c = J + 1$, where K_a and K_c are the usual asymmetric top quantum numbers [48] (see also Refs. [26–28,43,47] for further explanation of the origin and symbols used in Equation (1)).

The molecular symmetry group of (HF)₂ and its implications on the classification of the level structure and the electric dipole selection rules was subject of early studies by Dyke, Howard and Klempner [49] and by Hougen and Ohashi [50] and a detailed discussion in relation to the analysis of the far-infrared spectra has been given in Refs. [26–28,47]. We follow here Refs. [26,47] and the notation defined in [51] and give for definiteness the relevant character tables in Table 1 (see also Refs. [5,6,52]). There is experimental and theoretical evidence for the *trans tunneling path* to be dominant with a C_{2h} saddle point or transition state structure and low barrier of about 350 cm⁻¹ [7,28]. The group theoretical scheme for this path is therefore adequate and the corresponding approximate point group notation for C_{2h} has been frequently used [50], which we give here in parentheses. It should be noted, however, that the classification

Table 1. Character tables for the symmetry groups of the HF dimer ($H^{(1)}F^{(2)} H^{(3)}F^{(4)}$) [5,6,26].

(a) Character table and species of the molecular symmetry group M_{S_4} of (HF)₂. The approximate point group (C_{2h}) species notation is given in parentheses (see also Refs. [52,54,55] and references cited therein for conventions and notation).

Species	E	E^*	$(ab) (13)(24)$	$(ab)^* (13)(24)^*$	$\Gamma(M_{S_4}) \uparrow S_{2,2}^*$
$A^+ (A_g)$	1	1	1	1	$A_1^+ + A_2^+$
$A^- (A_u)$	1	-1	1	-1	$A_1^- + A_2^-$
$B^+ (B_g)$	1	1	-1	-1	$B_1^+ + B_2^+$
$B^- (B_u)$	1	-1	-1	1	$B_1^- + B_2^-$

(b) Character table and symmetry species for $S_{2,2}$.

Species	E	(13)	(24)	(13)(24)	$(S_{2,2}) \downarrow M_{S_2}$
$A \times A \equiv A_1$	1	1	1	1	A
$B \times B \equiv A_2$	1	-1	-1	1	A
$B \times A \equiv B_1$	1	-1	1	-1	B
$A \times B \equiv B_2$	1	1	-1	-1	B

of eigenstates with symmetry labels from the molecular symmetry group M_{S_4} of permutation-inversion operations is independent of any assumption of the tunneling path, as tunneling is in any case multidimensional. For symmetry considerations we can assume the total (rovibrational-tunneling-nuclear spin) wavefunctions to be given by product-wavefunctions $\Psi_{\text{total}} = \psi_{rtv} \psi_n$ with $\psi_{rtv} = \psi_r \psi_t \psi_v$. The ‘tunneling mode’ is the disrotatory in-plane bending vibration ν_5 , for which a number of tunneling and K -sublevels were observed and analysed already in 1990 [53], where also a survey of the low energy level structure of HFHF is given. The symmetry of the tunneling wavefunctions, Γ_t , is either A^+ or B^+ , the symmetry of the vibrational wavefunctions, Γ_v , is A^+ for ν_2, ν_3 and ν_4 , B^+ for ν_1 and A^- for ν_6 , and the symmetry of the rotational wavefunctions Γ_r is A^+ (even K_c) or B^- (odd K_c). The symmetry of the nuclear spin wavefunctions, Γ_n , is either A^+ or B^+ . The allowed combinations are determined by the generalised Pauli principle, which requires $\Gamma_{\text{total}} = \Gamma_r \Gamma_t \Gamma_v \Gamma_n = A^+$ or A^- . The nuclear spin statistical weights g_i of Γ_n are $g_B = 6$ and $g_A = 10$, as the A species are symmetric with respect to monomer exchange and the B species are antisymmetric. The superscript indicates parity (‘+’, positive, symmetric with respect to inversion at the origin, or ‘-’, negative, antisymmetric with respect to inversion). We give also the induced representation for the full permutation-inversion group in the last column of Table 1 (see also [51,52] for an in-depth discussion of the symmetry aspects).

For allowed electric dipole moment transitions the following selection rules hold: $\Delta J = 0, \pm 1$ and $+ \Leftrightarrow -$ (change of parity); $A \Leftrightarrow A$ and $B \Leftrightarrow B$ for Γ_n (nuclear spin symmetry conservation) and therefore for Γ_{rtv} . Since (HF)₂ is nearly a prolate symmetric top, we have in addition approximate selection rules for the quantum

number K ($= K_a$): $\Delta K = 0$, giving rise to parallel bands (μ_a transition moment), or $\Delta K = \pm 1$, giving rise to perpendicular bands (μ_b or μ_c transition moment). The in-plane fundamentals ν_1 , ν_2 , ν_3 and ν_4 give rise to a , b -hybrid bands ($\Delta K = 0, \pm 1$), the out-of-plane fundamental ν_6 to a type c band ($\Delta K = \pm 1$). In the case of the in-plane fundamentals with A^+ symmetry, the upper and lower tunneling states involved must belong to different symmetry species A^+ and B^+ . This is in contrast to ν_6 where the two tunneling sublevels connected by the transition must belong to the same symmetry species. Figure 1 illustrates the selection rules for the two subbands the present investigation is concerned with. In the case of the ν_3 subband, the Q-branch transitions start from the higher component of K_c -doublets, in contrast to the P - and R -branch transitions which start from the lower component. For the ν_6 subband, the reverse is true.

4. Results, analysis and assignments

4.1. The $K_a = 0 \leftarrow 1$ subband of ν_6

The line-structure of two Q-branches near 380 cm^{-1} had been analysed and tentatively assigned in a previous investigation at our laboratory early on [26]. At that time, the assignment of the J quantum numbers was not unambiguous, however, and the corresponding P - and R -branch transitions had not been identified. The assignment of vibrational-tunneling quantum numbers as well as of K_a quantum numbers was therefore not uniquely possible, neither for the lower nor the upper states. Nevertheless, already then the first option of several possible assignments mentioned was the $K_a = 0 \leftarrow 1$ transition in ν_6 , which we confirm here. However, in 1987 other optional assignments could not be excluded [26].

The new spectra yield more accurate peak wavenumbers and a more extended range of valuable Q-branch lines. From a plot of wavenumber-differences of adjacent Q-branch peaks we established a hypothetical J -assignment. Predictions based on the SO-3 potential energy surface [29,56] favour the assignment to the two tunneling components of the $K_a = 0 \leftarrow 1$ subband of the ν_6 fundamental. Since the spectroscopic constants of the $K_a = 1$ ground state levels are very accurately known [28], we tested this hypothesis by means of combination differences. Using lower state energies as given by Equation (1), combination differences for the two tunneling components of this ν_6 subband can be expressed as follows:

$${}^P R_1(J-1) - {}^P P_1(J+1) = E_{01}^{(+)}(J+1) - E_{01}^{(+)}(J-1) \quad (2)$$

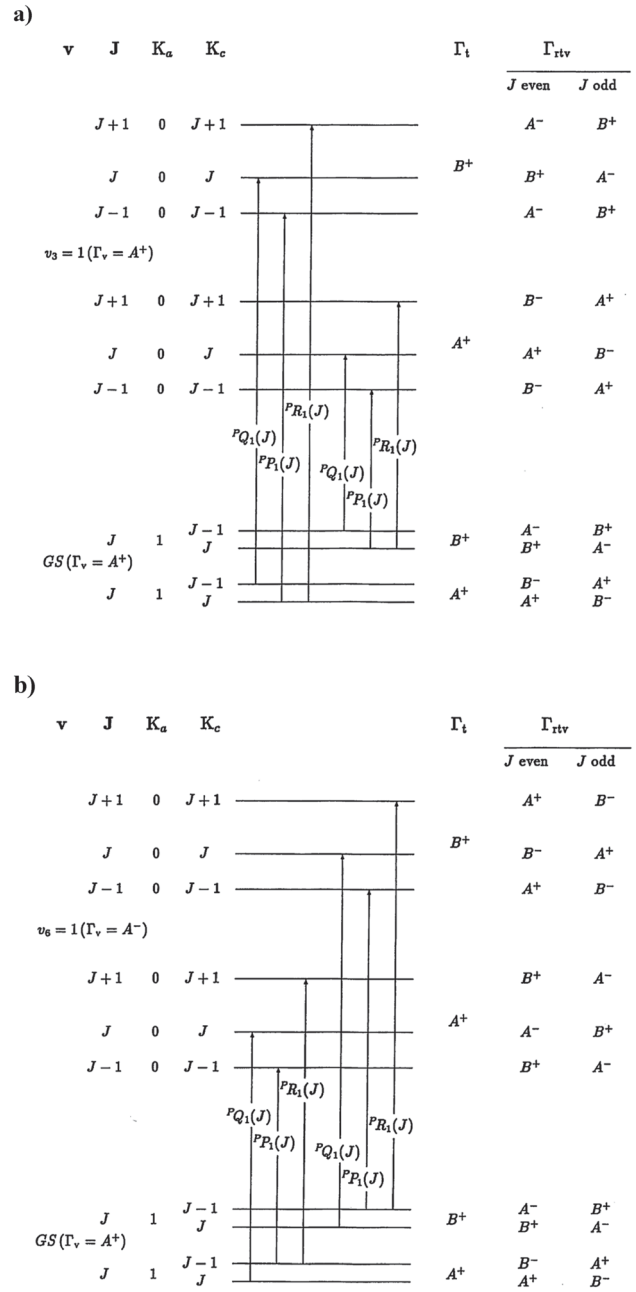


Figure 1. Schematic representation of the allowed transitions for the $K_a = 0 \leftarrow 1$ subbands of ν_3 (a) and ν_6 (b). Γ_t and Γ_v refer to the tunneling and vibrational states involved, and Γ_{rtv} is the overall species ('motional', rotation-vibration species apart from nuclear spin symmetry [52]).

$${}^P Q_1(J) - {}^P P_1(J+1) = E_{01}^{(+)}(J+1) - E_{01}^{(-)}(J) \quad (3)$$

$${}^P R_1(J-1) - {}^P Q_1(J) = E_{01}^{(-)}(J) - E_{01}^{(+)}(J-1) \quad (4)$$

We used Equations (3) and (4) to predict the P - and R -progressions belonging to the tentatively assigned Q-structure. By this procedure we were able to identify P -

and R -branch transitions and to definitely identify the lower state labels. Using the intensity alternation due to the nuclear spin weights as a further indication, we could verify the symmetry species of the upper vibrational state to be A^- and therefore definitely assign these subband structures to the $A^- \leftarrow A^+$ and $B^- \leftarrow B^+$ components of the $K_a = 0 \leftarrow 1$ subband of the fundamental ν_6 . We determined upper state constants according to equation (1) by a least squares fit. We omitted critical data when strong overlapping with neighbouring structures occurred and limited the input to transitions with lower state J quantum numbers smaller than 34. The reason for this restriction were systematic deviations of the residuals for larger J quantum numbers. The adjusted parameters and details of the statistics of the fit are listed in Table 2. Table 3 contains a listing of the observed transition wavenumbers used in the fit as well as the difference Δ between observed and calculated values (in $\text{cm}^{-1}/10^{-3}$). Figure 2 compares experimental and simulated survey spectra of this subband, and Figure 3 illustrates the region of the Q -branch origins on an expanded scale.

4.2. The $K_a = 0 \leftarrow 1$ subband of ν_3

Theoretical 6D-calculations based on the SO-3 potential energy surface [57–59] predict the tunneling sublevels of the symmetric bending vibration ν_3 at 483.54 cm^{-1} (A^+ tunneling component) and 486.12 cm^{-1} (B^+). According to the dipole selection rules, we expect an ab -hybrid band for this fundamental. The dipole component μ_b gives rise to a perpendicular band with a widely spaced and therefore well separated K -structure. Using the calculated values given above and ground state levels from [28], the centers of the tunneling components of the $K = 0 \leftarrow 1$ subband of ν_3 are predicted at 447.05 cm^{-1} ($A^+ \leftarrow B^+$ component) and at 450.70 cm^{-1} ($B^+ \leftarrow A^+$ component). The measured spectrum shown in Figure 4 reveals an accumulation of features in the region around 450 cm^{-1} . By comparing spacings between neighbouring lines we were able to identify two Q -branch progressions in this range. In the following we could assign corresponding P - and R -progressions by means of combination differences valid for the case of a $K_a = 0 \leftarrow 1$ subband of an A^+ fundamental, given by

$${}^P R_1(J-1) - {}^P P_1(J+1) = E_{01}^{(-)}(J+1) - E_{01}^{(-)}(J-1) \quad (5)$$

$${}^P Q_1(J) - {}^P P_1(J+1) = E_{01}^{(-)}(J+1) - E_{01}^{(+)}(J) \quad (6)$$

$${}^P R_1(J-1) - {}^P Q_1(J) = E_{01}^{(+)}(J) - E_{01}^{(-)}(J-1) \quad (7)$$

and thereby verify the identity of the lower states involved as well as the assignment of the rotational quantum

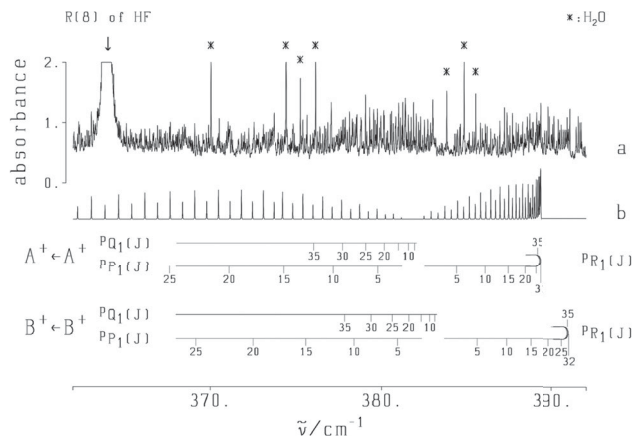


Figure 2. The $K_a = 0 \leftarrow 1$ subband of ν_6 of $(\text{HF})_2$. (a) Experimental spectrum (pressure = 20 mbar, temperature = 243 K, resolution apodized $\Delta\tilde{\nu}$ (FWHM) = 0.01 cm^{-1}), (b) simulated spectrum and assignments.

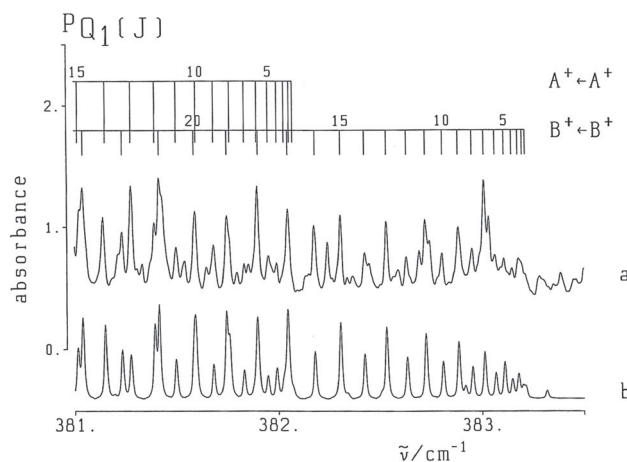


Figure 3. Low J part of the Q -branches of the two tunneling components of the $K_a = 0 \leftarrow 1$ subband of ν_6 . (a) Experimental spectrum, conditions see Figure 2. (b) simulated spectrum and assignments.

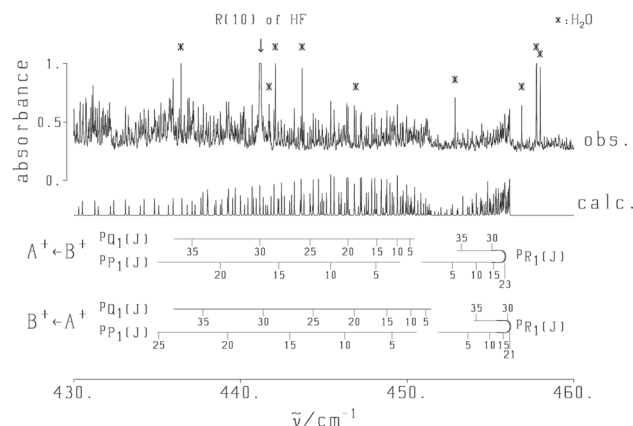
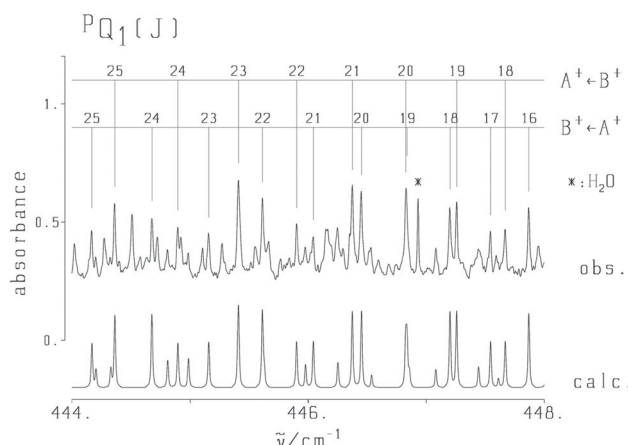
numbers. Furthermore the intensity alternation arising from nuclear spin statistical weights indicates the upper vibrational level belong to either the species A^+ or B^+ . The predicted values hardly leave any doubt that the upper vibrational state corresponds to ν_3 (A^+). The adjusted upper state constants are collected in Table 2. Again we excluded data which are problematic due to overlapping lines and restricted the least-squares fit to transitions with lower state J quantum numbers smaller than 34 for the same reasons as discussed above with the corresponding ν_6 subband. The transition wavenumbers used in the fit are listed in Table 4. Figure 4 shows experimental and simulated survey spectra of this subband, together with assignments, and Figure 5 illustrates a characteristic part of the Q -branch region in more detail.

Table 2. Spectroscopic parameters for the $K_a = 0 \leftarrow 1$ subbands of the fundamentals ν_3 and ν_6 of (HF)₂.

	ν_3		ν_6	
	A^+	B^+	A^+	B^+
Γ_t	A^+	B^+	A^+	B^+
Γ_{tv}	A^+	B^+	A^-	B^-
$\Delta\tilde{\nu}_0^{(a)} / \text{cm}^{-1}$	450.4546(8)	451.4583(6)	382.0802(6)	383.2245(4)
$\tilde{\nu}_{v_0}^{(b)} / \text{cm}^{-1}$	486.9442	486.8834	417.5053	419.7140
$\tilde{B}_{v_0} / \text{cm}^{-1}$	0.208894(10)	0.207288(7)	0.212695(5)	0.213222(4)
$D_{v_0} / 10^{-6} \text{cm}^{-1}$	1.435(37)	1.009(18)	2.1990(96)	2.3358(88)
$H_{v_0} / 10^{-10} \text{cm}^{-1}$	-11.43(37)	-5.48(12)	-0.767(56)	-0.645(53)
<i>Statistics of the fit:</i>				
number of data	45	54	52	63
J_{max}	28	31	36	34
$d_{\text{rms}} / 10^{-3} \text{cm}^{-1}$	1.75	1.74	1.45	1.33
<i>Ground state combination differences^(c):</i>				
number of differences	29	33	43	34
$d_{\text{rms}} / 10^{-3} \text{cm}^{-1}$	1.95	1.93	1.93	1.91
Ground state parameters for $K_a = 1$ [28]:				
Γ_t	A^+		B^+	
$\tilde{B}_{01} / \text{cm}^{-1}$	0.217860181		0.217709222	
$D_{01} / 10^{-6} \text{cm}^{-1}$	1.98814		1.96985	
$H_{01} / 10^{-12} \text{cm}^{-1}$	-39.27		-40.85	
$b_{01} / 10^{-3} \text{cm}^{-1}$	3.175940		3.041534	
$d_{01} / 10^{-9} \text{cm}^{-1}$	-42.591		-36.913	

(a) Center of $K_a = 0 \leftarrow 1$ subband tunneling component;(b) term value with respect to ground state $K_a = 0, A^+$ term;

(c) statistics of prediction using ground state parameters from Ref. [28].

**Figure 4.** The $K_a = 0 \leftarrow 1$ subband of ν_3 of (HF)₂. (a) Experimental spectrum (pressure = 20 mbar, temperature = 243 K, resolution apodized $\Delta\tilde{\nu}$ (FWHM) = 0.01 cm⁻¹), (b) simulated spectrum and assignments.**Figure 5.** Details of the Q -branches of the two tunneling components of the $K_a = 0 \leftarrow 1$ subband of ν_3 . (a) Experimental spectrum, conditions see Figure 4. (b) Simulated spectrum and assignments.

5. Discussion of the results and comparison with theory

The analysis of the two $K_a = 0 \leftarrow 1$ subbands provide accurate term values of both tunneling components of the fundamentals ν_3 and ν_6 . The fits based on the term formula given by Equation (1) which includes contributions up to the sixth power in J approaches the experimental accuracy. For transitions with $J'' > J_{\text{max}}$ systematic deviations occur. We consider this deficiency to be an indication for the limited validity of the theoretical model used. Due to the high flexibility of this molecule interactions

between internal motion and rotation may become very strong for higher J quantum numbers and can hardly be described by a term formula appropriate for quasi-rigid molecules.

The identification of the lower states involved in the transitions of these subbands is based on combination differences. For both tunneling components of both subbands investigated, a representative number of ground state combination differences could be formed. Using accurate ground state parameters from Ref. [28], these

Table 3. Rovibrational Tunneling Transitions of the $K_a = 0 \leftarrow 1$ subband of ν_6 of $(\text{HF})_2$.

Γ'_t	J'	K'_c	Γ_t	J	K_c	$\tilde{\nu}_{\text{obs}} / \text{cm}^{-1}$	$\Delta / 10^{-3}$
Q-branch transitions:							
A^+	4	4	A^+	4	4	381.9929	0.19
A^+	7	7	A^+	7	7	381.8358	1.14
A^+	9	9	A^+	9	9	381.6850	0.23
A^+	10	10	A^+	10	10	381.5924	-3.91
A^+	11	11	A^+	11	11	381.4987	-0.07
A^+	12	12	A^+	12	12	381.3905	-1.56
A^+	16	16	A^+	16	16	380.8721	0.26
A^+	17	17	A^+	17	17	380.7184	0.47
A^+	18	18	A^+	18	18	380.5543	0.05
A^+	19	19	A^+	19	19	380.3807	0.06
A^+	20	20	A^+	20	20	380.1959	-1.08
A^+	22	22	A^+	22	22	379.7987	-0.13
A^+	24	24	A^+	24	24	379.3578	-0.59
A^+	26	26	A^+	26	26	378.8744	0.36
A^+	27	27	A^+	27	27	378.6143	-0.54
A^+	28	28	A^+	28	28	378.3452	1.25
A^+	29	29	A^+	29	29	378.0601	-1.02
A^+	30	30	A^+	30	30	377.7658	-0.24
A^+	31	31	A^+	31	31	377.4586	0.18
B^+	4	4	B^+	4	4	383.1514	1.61
B^+	5	5	B^+	5	5	383.1113	-1.02
B^+	6	6	B^+	6	6	383.0669	-0.35
B^+	8	8	B^+	8	8	382.9545	0.44
B^+	9	9	B^+	9	9	382.8867	0.90
B^+	10	10	B^+	10	10	382.8074	-2.24
B^+	11	11	B^+	11	11	382.7250	-0.48
B^+	12	12	B^+	12	12	382.6320	-1.22
B^+	13	13	B^+	13	13	382.5331	0.37
B^+	14	14	B^+	14	14	382.4256	1.71
B^+	15	15	B^+	15	15	382.3071	0.56
B^+	16	16	B^+	16	16	382.1765	-4.03
B^+	17	17	B^+	17	17	382.0473	1.59
B^+	22	22	B^+	22	22	381.2321	-0.46
B^+	23	23	B^+	23	23	381.0396	-1.01
B^+	24	24	B^+	24	24	380.8400	1.68
B^+	25	25	B^+	25	25	380.6244	-1.03
B^+	26	26	B^+	26	26	380.4001	-1.53
B^+	27	27	B^+	27	27	380.1651	-1.54
B^+	28	28	B^+	28	28	379.9210	0.87
B^+	29	29	B^+	29	29	379.6617	-0.07
B^+	30	30	B^+	30	30	379.3918	0.58
B^+	32	32	B^+	32	32	378.8132	1.16
B^+	33	33	B^+	33	33	378.5018	-0.82
P-branch transitions:							
A^+	5	5	A^+	6	5	379.2790	-0.22
A^+	6	6	A^+	7	6	378.7733	2.01
A^+	9	9	A^+	10	9	377.1772	-0.40
A^+	10	10	A^+	11	10	376.6257	2.58
A^+	11	11	A^+	12	11	376.0540	-3.04
A^+	12	12	A^+	13	12	375.4787	-0.63
A^+	16	16	A^+	17	16	373.0529	0.68
A^+	17	17	A^+	18	17	372.4174	1.14
A^+	18	18	A^+	19	18	371.7681	-0.46
A^+	19	19	A^+	20	19	371.1094	0.31
A^+	20	20	A^+	21	20	370.4377	-0.07
A^+	21	21	A^+	22	21	369.7556	1.04
A^+	22	22	A^+	23	22	369.0595	0.12
A^+	23	23	A^+	24	23	368.3522	0.05
A^+	25	25	A^+	26	25	366.8978	-3.37
A^+	26	26	A^+	27	26	366.1599	2.70
A^+	27	27	A^+	28	27	365.3985	-2.25
A^+	28	28	A^+	29	28	364.6336	1.91
A^+	31	31	A^+	32	31	362.2470	-0.19
A^+	32	32	A^+	33	32	361.4268	0.82
A^+	34	34	A^+	35	34	359.7424	-0.37
B^+	1	1	B^+	2	1	382.3395	-0.68
B^+	4	4	B^+	5	4	380.9376	1.87
B^+	5	5	B^+	6	5	380.4476	0.72

(continued).

Table 3. Continued.

Γ'_t	J'	K'_c	Γ_t	J	K_c	$\tilde{\nu}_{\text{obs}} / \text{cm}^{-1}$	$\Delta / 10^{-3}$
<i>P</i> -branch transitions:							
B^+	6	6	B^+	7	6	379.9444	-3.32
B^+	7	7	B^+	8	7	379.4385	0.27
B^+	8	8	B^+	9	8	378.9188	0.39
B^+	9	9	B^+	10	9	378.3893	1.05
B^+	11	11	B^+	12	11	377.2949	-1.87
B^+	12	12	B^+	13	12	376.7350	-0.39
B^+	14	14	B^+	15	14	375.5809	-0.20
B^+	15	15	B^+	16	15	374.9883	0.24
B^+	16	16	B^+	17	16	374.3833	-1.03
B^+	17	17	B^+	18	17	373.7691	-0.72
B^+	19	19	B^+	20	19	372.5079	-0.17
B^+	20	20	B^+	21	20	371.8617	1.09
B^+	21	21	B^+	22	21	371.2023	0.37
B^+	22	22	B^+	23	22	370.5331	1.21
B^+	23	23	B^+	24	23	369.8502	-0.15
B^+	24	24	B^+	25	24	369.1576	0.47
B^+	25	25	B^+	26	25	368.4526	0.52
B^+	26	26	B^+	27	26	367.7364	1.40
B^+	27	27	B^+	28	27	367.0066	0.90
B^+	28	28	B^+	29	28	366.2636	-0.38
B^+	29	29	B^+	30	29	365.5089	-0.70
B^+	30	30	B^+	31	30	364.7416	-0.73
B^+	32	32	B^+	33	32	363.1660	-2.10
B^+	33	33	B^+	34	33	362.3625	1.90
<i>R</i> -branch transitions:							
A^+	16	16	A^+	15	14	387.4104	0.77
A^+	18	18	A^+	17	16	387.8477	2.85
A^+	19	19	A^+	18	17	388.0430	0.93
A^+	20	20	A^+	19	18	388.2258	0.31
A^+	21	21	A^+	20	19	388.3937	-1.22
A^+	22	22	A^+	21	20	388.5486	-1.60
A^+	23	23	A^+	22	21	388.6905	-0.63
A^+	24	24	A^+	23	22	388.8175	0.00
A^+	25	25	A^+	24	23	388.9299	0.80
A^+	26	26	A^+	25	24	389.0281	2.39
A^+	27	27	A^+	26	25	389.1049	-2.17
A^+	28	28	A^+	27	26	389.1731	0.16
B^+	5	5	B^+	4	3	385.2487	-1.76
B^+	6	6	B^+	5	4	385.6255	2.08
B^+	8	8	B^+	7	6	386.3369	0.53
B^+	9	9	B^+	8	7	386.6786	2.45
B^+	10	10	B^+	9	8	387.0048	0.16
B^+	13	13	B^+	12	11	387.9204	-0.57
B^+	19	19	B^+	18	17	389.4290	1.01
B^+	22	22	B^+	21	20	390.0097	1.57
B^+	24	24	B^+	23	22	390.3255	-0.86
B^+	25	25	B^+	24	23	390.4646	0.49
B^+	27	27	B^+	26	25	390.6942	-1.16
B^+	29	29	B^+	28	27	390.8659	0.44

combination differences can be predicted very accurately. As summarised in Table 2, the rms-deviations amount to about $d_{\text{rms}} = 0.0019 \text{ cm}^{-1}$ for all of the four subband-tunneling components analyzed. This value compares well with the experimental uncertainty, which amounts to 0.0012 cm^{-1} for a single transition, and therefore $0.0012 \sqrt{2} \approx 0.0017 \text{ cm}^{-1}$ for the difference of two transitions. In view of this good consistency, the identity of the lower state assignments is strongly confirmed.

In Figures 2 and 4 we compare measured and calculated spectra. The clearly smaller \bar{B} constants in the excited ν_3 and ν_6 states as compared to the ground state

lead to band heads in the *R*-branches of all subband-tunneling components. In the case of ν_3 the branch turns near $J'' \approx 20$, and in the case of ν_6 at a higher value of $J'' \approx 30$. The details of the *Q*-branches shown in Figures 3 and 5 demonstrate the excellent agreement between experimental and calculated spectra. The intensity alternation arising from the nuclear spin statistical weights is unambiguously established and confirms the assignment of the symmetry of the vibrational-tunneling states involved. The figures also show that there still remains a considerable amount of structure in these regions which does not belong to the identified subbands. The centrifugal distortion constants D_{ν_0} differ

Table 4. Rovibrational tunneling transitions of the $K_a = 0 \leftarrow 1$ subband of ν_3 of $(\text{HF})_2$.

Γ'_t	J'	K'_c	Γ_t	J	K_c	$\tilde{\nu}_{\text{obs}} / \text{cm}^{-1}$	$\Delta / 10^{-3}$
Q-branch transitions:							
A^+	4	4	B^+	4	3	450.2603	-3.02
A^+	5	5	B^+	5	4	450.1723	4.47
A^+	6	6	B^+	6	5	450.0517	-1.67
A^+	7	7	B^+	7	6	449.9220	2.02
A^+	8	8	B^+	8	7	449.7669	-0.82
A^+	9	9	B^+	9	8	449.5986	1.96
A^+	11	11	B^+	11	10	449.1997	1.64
A^+	12	12	B^+	12	11	448.9729	2.35
A^+	13	13	B^+	13	12	448.7248	0.66
A^+	14	14	B^+	14	13	448.4593	0.56
A^+	15	15	B^+	15	14	448.1741	-0.06
A^+	16	16	B^+	16	15	447.8706	0.44
A^+	17	17	B^+	17	16	447.5457	-0.72
A^+	18	18	B^+	18	17	447.2019	-0.63
A^+	20	20	B^+	20	19	446.4511	-0.93
A^+	21	21	B^+	21	20	446.0441	0.10
A^+	22	22	B^+	22	21	445.6146	1.68
A^+	23	23	B^+	23	22	445.1581	0.43
A^+	24	24	B^+	24	23	444.6780	1.04
A^+	25	25	B^+	25	24	444.1685	-0.79
B^+	3	3	A^+	3	2	451.3265	4.48
B^+	4	4	A^+	4	3	451.2332	1.85
B^+	5	5	A^+	5	4	451.1192	1.02
B^+	6	6	A^+	6	5	450.9816	-1.05
B^+	7	7	A^+	7	6	450.8269	2.03
B^+	8	8	A^+	8	7	450.6466	1.60
B^+	9	9	A^+	9	8	450.4414	-1.80
B^+	10	10	A^+	10	9	450.2170	-2.65
B^+	12	12	A^+	12	11	449.7076	-0.45
B^+	15	15	A^+	15	14	448.7818	-0.36
B^+	16	16	A^+	16	15	448.4322	0.23
B^+	17	17	A^+	17	16	448.0619	0.64
B^+	18	18	A^+	18	17	447.6701	-0.03
B^+	19	19	A^+	19	18	447.2600	1.32
B^+	21	21	A^+	21	20	446.3756	0.67
B^+	22	22	A^+	22	21	445.9040	1.40
B^+	23	23	A^+	23	22	445.4110	1.18
B^+	24	24	A^+	24	23	444.8969	0.48
B^+	25	25	A^+	25	24	444.3613	-0.85
B^+	26	26	A^+	26	25	443.8046	-2.06
B^+	27	27	A^+	27	26	443.2276	-1.92
B^+	28	28	A^+	28	27	442.6273	-2.89
B^+	29	29	A^+	29	28	442.0069	-1.12
B^+	30	30	A^+	30	29	441.3622	-0.02
B^+	31	31	A^+	31	30	440.6948	2.92
P-branch transitions:							
A^+	4	4	B^+	5	5	448.1219	-3.29
A^+	5	5	B^+	6	6	447.6105	-1.17
A^+	6	6	B^+	7	7	447.0842	1.72
A^+	8	8	B^+	9	9	445.9769	-0.51
A^+	10	10	B^+	11	11	444.8100	-0.59
A^+	11	11	B^+	12	12	444.2024	-1.76
A^+	12	12	B^+	13	13	443.5849	2.50
A^+	14	14	B^+	15	15	442.2919	-0.76
A^+	15	15	B^+	16	16	441.6242	-0.25
A^+	16	16	B^+	17	17	440.9418	1.38
A^+	17	17	B^+	18	18	440.2380	-2.26
A^+	18	18	B^+	19	19	439.5218	-1.78
A^+	20	20	B^+	21	21	438.0367	-1.79
A^+	21	21	B^+	22	22	437.2689	0.21
A^+	23	23	B^+	24	24	435.6725	2.57
A^+	24	24	B^+	25	25	434.8392	0.59
B^+	5	5	A^+	6	6	448.5644	1.76
B^+	6	6	A^+	7	7	448.0138	0.86
B^+	7	7	A^+	8	8	447.4442	-0.26
B^+	9	9	A^+	10	10	446.2505	-1.41

(continued).

Table 4. Continued.

Γ'_t	J'	K'_c	Γ_t	J	K_c	$\tilde{\nu}_{\text{obs}} / \text{cm}^{-1}$	$\Delta / 10^{-3}$
<i>P</i> -branch transitions:							
B^+	11	11	A^+	12	12	444.9853	-1.29
B^+	12	12	A^+	13	13	444.3235	-3.66
B^+	17	17	A^+	18	18	440.7727	2.05
B^+	19	19	A^+	20	20	439.2322	2.03
B^+	20	20	A^+	21	21	438.4366	1.48
B^+	21	21	A^+	22	22	437.6238	0.24
B^+	22	22	A^+	23	23	436.7977	2.24
B^+	25	25	A^+	26	26	434.2108	0.32
B^+	26	26	A^+	27	27	433.3167	2.28
B^+	27	27	A^+	28	28	432.3989	-1.63
B^+	29	29	A^+	30	30	430.5172	0.25
B^+	30	30	A^+	31	31	429.5446	-1.24
<i>R</i> -branch transitions:							
A^+	12	12	B^+	11	11	454.3997	0.36
A^+	13	13	B^+	12	12	454.6199	-2.17
A^+	14	14	B^+	13	13	454.8288	0.74
A^+	15	15	B^+	14	14	455.0189	1.83
A^+	16	16	B^+	15	15	455.1872	-1.58
A^+	18	18	B^+	17	17	455.4779	-0.70
A^+	20	20	B^+	19	19	455.6909	-2.15
A^+	22	22	B^+	21	21	455.8276	1.92
A^+	26	26	B^+	25	25	455.8049	-1.76
B^+	7	7	A^+	6	6	453.9487	-1.08
B^+	8	8	A^+	7	7	454.2250	-2.96
B^+	10	10	A^+	9	9	454.7234	-3.42
B^+	11	11	A^+	10	10	454.9483	0.57
B^+	12	12	A^+	11	11	455.1488	-0.98
B^+	13	13	A^+	12	12	455.3335	0.41
B^+	15	15	A^+	14	14	455.6432	-0.71
B^+	18	18	A^+	17	17	455.9721	0.30
B^+	19	19	A^+	18	18	456.0446	0.24
B^+	21	21	A^+	20	20	456.1323	-1.84
B^+	26	26	A^+	25	25	456.0269	-0.40
B^+	29	29	A^+	28	28	455.7203	0.02
B^+	30	30	A^+	29	29	455.5747	1.22

considerably from the ground state values. They also differ strongly for the different tunneling components. The values of the sextic constants vary even more strongly. We consider this to be an indication for a stronger influence of the flexibility of this molecule in the vibrationally excited states. As one can hardly give a simple physical interpretation for these parameters, we consider them primarily as effective fitting variables, which do, however, allow for a compact and accurate representation of the experimental energy level structure of HFHF.

Table 5 shows a comparison of experimental and calculated vibrational-tunneling term values for various types of potential energy surfaces and approximations. Whereas predictions based on the SQSBDE potential energy surface [4,39] are considerably off, we find rather good agreement for the more recent calculations based on the SO-3 surface [29,56,57] and on the most recent HYZX [30] and RPB surfaces [31] which, however, give even a little less good predictions than the SO-3 surface of [29], which still can be considered to be the ‘best compromise’ potential hypersurface. Concerning the tunneling splitting, the agreement is generally excellent in the case of the out-of-plane fundamental

ν_6 , but differs in part considerably in the case of ν_3 , where we observe a very small negative shift. In the region of ν_3 , the density of bound states having symmetry A^+ or B^+ as also the tunneling components of ν_3 , is much higher than in the region of ν_6 . In particular, there are 5 additional bound states with $\Gamma_{vt} = A^+$ or B^+ in the interval 400–550 cm^{-1} , one of them being in near coincidence with the corresponding tunneling level of ν_3 (an A^+ state at 478.32 cm^{-1} , 6D calculation, and a B^+ state at 481.78 cm^{-1} , respectively, both representing highly excited FF-stretching states). A small change in the form of the potential energy surface is therefore expected to have a strong effect on the mixing of zeroth-order states and therefore on the tunneling splittings which may strongly depend on this composition. The present result for ν_6 also confirms the unusual sequence of the levels for $K_a = 0$ and 1, the level for $K_a = 0$ lying above the one for $K_a = 1$. This agrees with the calculations on the SO-3 surface. This unusual level sequence was already surmised in 1987 in our early work [26] as a realistic possibility due to Coriolis coupling and was traced to strong a -axis Coriolis interaction between the in- and out-of-plane bending modes in [29]. This special situation for

Table 5. Comparison of experimental and calculated term values and tunneling splittings (in cm^{-1}) for $K_a = 0$. The term values are relative to the ground state A^+ tunneling level.

Vibration	Γ_t	Experimental	SO-3 ^(a) 6D Refs. [6,57]	SO-3 (4+2)D Ref. [56]	SQSBDE 6D Refs. [4,39] ^(b)	HYZX 6D Ref. [30]	RPB 6D Ref. [31]
ν_3	A^+	486.9442	483.48	482.73	425.30	481.647	490.5 (484.4) ^(c)
	B^+	486.8834	486.12	485.21	440.32	481.322	491.7
$\Delta\nu_t(\nu_3)$		-0.0608	2.65	2.48	15.02	-0.325	1.21
ν_6	A^+	417.5053	420.83	420.48	378.72	413.271	418.6 (418.4) ^(c)
	B^+	419.7140	423.10	422.84	380.47		
$\Delta\nu_t(\nu_6)$		2.2087	2.22	2.36	1.75	2.284	2.13

^(a) See also further references in [6] and Ref. [29] for the potential hypersurface;

^(b) See also [60] for differing results;

^(c) Ref. [31], values taken from the supplementary tables, the values in parentheses from the respective columns Pall in the tables of [31], including all corrections by calculating $\bar{\nu}_{\text{calc}} = \bar{\nu}_{\text{obs}} - \text{Pall}$.

$K_a = 1$ also shows up in the K_a dependence of the tunneling splitting as well as the rotational constant \bar{B} [26,27] which reveal local extrema at $K_a = 1$. We might mention here also approximate full-dimensional quantum results on SQSBDE, which differ slightly [60].

A $K_a = 0$ combination level experimentally known involving ν_3 is $\nu_1 + \nu_3$ [61]. An interesting question concerns the degree of additivity of spectroscopic parameters of the levels ν_1 and ν_3 to obtain estimates of corresponding quantities for the combination level. In particular we tested the additivity of the vibrational term values, of the tunneling-splittings and of the dependence of the rotational constants \bar{B} upon vibrational state ν expressed by the $\alpha_i^{\bar{B}}$ constants defined by [62]

$$\bar{B}_\nu = \bar{B}_e - \sum_i \alpha_i^{\bar{B}} \left(\nu_i + \frac{1}{2} \right) \quad (8)$$

The values collected in Table 6 reflect a high degree of additivity. The vibrational term values and tunneling splitting agree reasonably well. The very small cross anharmonicities between the intramolecular ν_1 mode on one hand and the intermolecular mode ν_3 on the other hand is not too surprising since ν_1 corresponds to the free HF stretching mode which obviously does not strongly influence the dynamics of the intermolecular (low-frequency) modes. In the case of the $\alpha_i^{\bar{B}}$ constants,

Table 6. Comparison of parameters of the combination level $\nu_1 + \nu_3$ with the sum of the corresponding parameters of the separate levels ν_1 and ν_3 listed in column ' ν_1 plus ν_3 '.

	Γ_t	ν_1 Ref. [47] ^(a)	ν_3 this work	ν_1 plus ν_3	$\nu_1 + \nu_3$ Ref. [61]
$\bar{\nu}_{\nu_0}$	A^+	3930.903	486.9442	4417.8472	4418.0629
	B^+	3931.118	486.8834	4418.0014	4417.9183
$\Delta\nu_t$		0.2150	-0.0608	0.1542	-0.1446
$\alpha_{\nu_0}^{\bar{B}}$	A^+	-0.001225	0.007819	0.006594	0.007453
	B^+	-0.001293	0.009287	0.007994	0.007705

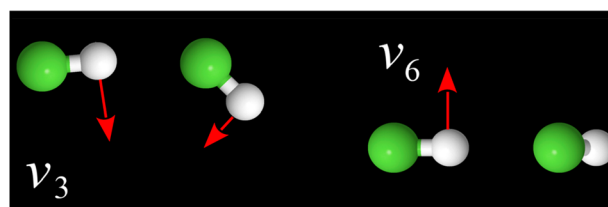
^(a) See also Ref. [63].

the additivity is less perfect although the tendency is clearly indicated.

6. Conclusions

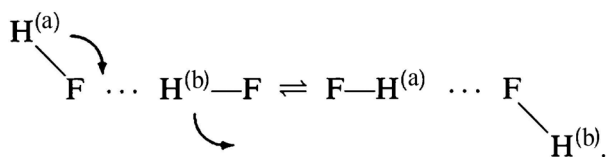
The present work has as main experimental result a first assignment and analysis of the $K = 0 \leftarrow 1$ transitions for the in-plane fundamental ν_3 and the out-of-plane fundamental ν_6 of the hydrogen bonded dimer (HFHF). Together with the very accurate knowledge of the $K = 1$ level in the vibrational ground state from our previous work [28,53], this provides highly accurate values for the purely vibrational term values (with $K = 0$) of the tunneling sublevels of these two fundamentals (see Table 5). For ν_6 this result agrees with a tentative assignment mentioned already in the very first investigation of high-resolution spectra of (HFHF) in the far infrared where an accurate term value for the $K = 1$ level of ν_6 was obtained [26]. However, based on the data available then, the assignment of the position of the $K = 0$ level of ν_6 remained ambiguous, allowing either for a 'high' value of ν_6 (the $K = 0$ level being then above the $K = 1$ level as found in the present work) or else for a 'low' value for the $\nu_6 = 1, K = 0$ level, below the $K = 1$ level of ν_6 . The new experimental results presented here establish the high value for ν_6 without ambiguity.

The situation was even more difficult for the fundamental ν_3 which resisted an accurate analysis for a long time. Again, both 'high' and 'low' values were discussed

**Figure 6.** Qualitative graphical representation of the vibrational modes ν_3 and ν_6 in (HFHF).

as possible alternatives for this fundamental. From the limited theoretical and experimental information available early on, we favoured a ‘high’ value, for instance in [43] (for the harmonic wavenumber ω_3 and by inference for ν_3). However, in the design of the later widely used full-dimensional SQSBDE potential hypersurface [4] a ‘low’ value for ν_3 (and for ω_3) resulted from a fit to low level *ab initio* potential points and some empirical adjustment. As the ambiguity was recognized already then, this led to several theoretical efforts with higher level *ab initio* calculations which all preferred ‘high’ values for ω_3 (and by inference for ν_3) [23,29,40,41]. Finally a whole group of newly designed full-dimensional potential hypersurfaces based on new high level *ab initio* results and some empirical adjustment provided predictions of the ‘high’ values for both ν_3 and ν_6 [7,23,29]. The present experimental results provide proof without ambiguity also for the ‘high’ values of ν_3 (Table 5). Figure 6 provides a qualitative picture of the motion related to these two vibrational modes, an in-plane and out-of-plane ‘bending’ mode, which most importantly involve displacements of the hydrogen atoms from the equilibrium geometry, with ν_3 corresponding to a conrotatory in-plane motion.

One might on the basis of the atomic motions in these vibrational modes address the question of mode-selective enhancement or inhibition of tunneling by vibrational excitation of ν_3 and ν_6 , which in a normal mode picture are separable from the in-plane disrotatory bending mode, which represents the tunneling mode for the hydrogen bond switching process,



As the electronic barrier at the C_{2h} saddle point along the switching path is about 350 cm^{-1} ($\pm 20\text{ cm}^{-1}$ according to a best estimate from [7], and 337 cm^{-1} in the SO-3 surface [29]) the excitation of either ν_3 or ν_6 with one quantum leads to quasiadiabatic channel above barrier tunneling [5,6,22] (see also the discussion on the fully anharmonic quasiadiabatic channel potential by Diffusion Quantum Monte Carlo methods [28]). The excitation of ν_6 leads to enhancement of tunneling (with tunneling splitting of 0.659 cm^{-1} in the ground state and 2.209 cm^{-1} in $\nu_6 = 1$), and all theoretical treatments summarized in Table 5 are consistent with this experimental result. On the other hand, the excitation of ν_3 leads to an inverted and in absolute value much reduced tunneling splitting (by the definition of $\Delta\tilde{\nu} = \tilde{\nu}_{B^+} - \tilde{\nu}_{A^+} = -0.061\text{ cm}^{-1}$, being then negative).

The theoretical splittings are variable, depending on the potential hypersurface used (one with negative $\Delta\tilde{\nu}$ and three with positive $\Delta\tilde{\nu}$ in Table 5), none of them being very close to the experimental result. This indicates very complex multidimensional dynamic effects on the tunneling, which one might interpret in terms of vibrationally non-adiabatic couplings with close lying ‘perturber’ states. This complex situation was already discussed for (HFHF) in [28,53] and furthermore there is a strong dependence of tunneling on the quantum number K . This behaviour is quite different from tunneling in HOOH and similar molecules, where tunneling can be well described with the quasiadiabatic channel reaction path Hamiltonian treatment [64–66]. However, complex vibrationally nonadiabatic effects are also found in the prototypical molecule NH_3 for inversion tunneling ([67] and references cited therein).

As part of a larger project of spectroscopic studies covering the whole infrared range from the far-infrared to the visible ranges [5–13,26–29,43,44,47,53,58,59,70] the present investigations of ν_3 and ν_6 aim also at providing benchmark results for *ab initio* calculations, which are, indeed, numerous for this prototypical hydrogen bonded dimer (see Refs. [23,29–36,40,41,68,69], this list being by no means complete). Furthermore the potential hypersurfaces based on the spectroscopic and *ab initio* results have also been used for benchmark studies of quantum eigenstate calculations. In this context notably the older SQSBDE potential [4] has been widely used as basis for such benchmark studies [8,38,39,56–58,60,70–83]. More recently also the improved potential SO-3 has been used as well by some authors [29,57–59,71,84,85]. We have shown in recent work completing the overtone HF-stretching polyad analyses to $N = 2$ in the near infrared that, indeed, SO-3 is able to reproduce well the experimental results [6,42,59]. For the recent *ab initio* surfaces [30,31] the $N = 2$ polyad overtone tunneling sublevels have not yet been computed. However, as summarized in Table 5 for ν_3 and ν_6 and more completely also for the other modes in Ref. [6], for the low frequency modes the SO-3 surface performs overall as well or even better than the most recent *ab initio* potentials. The dynamically very important hydrogen bond dissociation energy corresponding to $D_0 = 1062\text{ cm}^{-1}$ is perfectly represented by SO-3 (being adjusted to this value). There are still sizable differences in D_0 for the HYZX surface (Ref. [30], $D_0 = 1037.5\text{ cm}^{-1}$) and for the RPB surface (Ref. [31], $D_0 = 1065.6\text{ cm}^{-1}$). Thus we may conclude that in consideration of the present and previous results the SO-3 potential hypersurface can be considered to be the best compromise currently available for use in quantum dynamical calculations of HFHF.

We might mention also the significance of such spectroscopic experiments combined with full-dimensional theoretical benchmark results in relation to the quantum dynamics of hydrogen bonded clusters in general including the particularly important water clusters $(\text{H}_2\text{O})_n$ [86–91]. For instance, the early full-dimensional potential and quantum dynamical results for (HFHF) demonstrated the importance of a fully 6D treatment for the tunneling-rotation-vibration problem [4], as it showed large differences compared to the common reduced dimensional treatments with keeping the HF bond lengths as intramolecular degrees of freedom fixed [92]. Such reduced dimensional treatments with frozen intramolecular degrees of freedom were commonly used for more complex clusters such as $(\text{H}_2\text{O})_2$. The findings with full dimensional dynamics of $(\text{HF})_2$ motivated then full dimensional treatments also for $(\text{H}_2\text{O})_2$, showing important effects on the dimer properties [87–89], including the ground state dissociation energy D_0 as compared to the dissociation energy D_e from electronic structure theory for $(\text{H}_2\text{O})_2$ [91], as well as other eigenstate properties. In an even broader context the spectroscopic results for HFHF dynamics can be considered as simple prototypes for the dynamics of rotors in molecular machines [93,94] or for understanding hydrogen bonding in general [95–97].

Acknowledgements

Many years of friendly scientific exchange with Attila G. Császár are gratefully acknowledged, to whom this publication is thus justly dedicated. We are grateful to Katharina Al-Shamery (née v. Puttkamer), Jochen Blumberger, Yabei He, David Luckhaus, Carine Manca Tanner, Roberto Marquardt, Frédéric Merkt, Holger Müller, Ruth Signorell, Martin Suhm, Gunther Wichmann and Martin Willeke for help and discussions at various stages of our work and Zlatko Bačić for continuing collaboration on the theory of (HFHF) eigenstates and spectra, the results of which will be published elsewhere.

Disclosure statement

No potential conflict of interest was reported by the author(s).

Funding

Our work is supported financially by the ETH Zürich, the Schweizerischer Nationalfonds and the AGS project as well as COST MOLIM and COST COSY and an advanced grant from the ERC of the European Union. Michael Hippler acknowledges support by a visiting professorship at the ETH Zürich.

ORCID

M. Hippler  <http://orcid.org/0000-0002-3956-3922>

M. Quack  <http://orcid.org/0000-0002-1351-8584>

References

- [1] *Handbook of High Resolution Spectroscopy, 3 Volumes*, edited by M. Quack, F. Merkt (Wiley, Chichester, New York, 2011).
- [2] A.G. Császár, C. Fábri and T. Szidarovszky, Exact Numerical Methods for Stationary-State-Based Quantum Dynamics of Complex Polyatomic Molecules, Chapter 2, in *Molecular Spectroscopy and Quantum Dynamics*, edited by R. Marquardt, M. Quack (Elsevier, Amsterdam, St Louis, 2021). pp. 43–78.
- [3] A.G. Császár, C. Fábri, T. Szidarovszky, E. Mátyus, T. Furtenbacher and G. Czako, *Phys. Chem. Chem. Phys.* **14**, 1085–1106 (2012). doi: [10.1039/C1CP21830A](https://doi.org/10.1039/C1CP21830A)
- [4] M. Quack and M.A. Suhm, *J. Chem. Phys.* **95**, 28–59 (1991). doi: [10.1063/1.461486](https://doi.org/10.1063/1.461486)
- [5] M. Quack and G. Seyfang, Atomic and Molecular Tunneling Processes in Chemistry, Chapter 7, in *Molecular Spectroscopy and Quantum Dynamics*, edited by R. Marquardt, M. Quack (Elsevier, Amsterdam, St Louis, 2021). pp. 231–282. doi: [10.1016/B978-0-12-817234-6.00012-X](https://doi.org/10.1016/B978-0-12-817234-6.00012-X)
- [6] M. Hippler, L. Oeltjen and M. Quack, *Isr. J. Chem.* **63**, e202300092 (2023). doi: [10.1002/ijch.202300092](https://doi.org/10.1002/ijch.202300092)
- [7] M. Quack and M.A. Suhm, Potential Energy Hyper-surfaces for Hydrogen Bonded Clusters $(\text{HF})_n$, in *Conceptual Perspectives in Quantum Chemistry*, edited by E.S. Kryachko, J.L. Calais (Kluwer, Dordrecht, 1997). pp. 415–463.
- [8] M. Quack and M.A. Suhm, Spectroscopy and Quantum Dynamics of Hydrogen Fluoride Clusters, in *Advances in Molecular Vibrations and Collision Dynamics, Vol. III Molecular Clusters*, edited by Z. Bačić, J. Bowman (JAI Press, Stamford, Conn., 1998). pp. 205–248.
- [9] R. Marquardt and M. Quack, Global Analytical Potential Energy Surfaces for High Resolution Spectroscopy and Reaction Dynamics, Chapter 12, in *Handbook of High Resolution Spectroscopy, Vol. 1*, edited by M. Quack, F. Merkt (Wiley, Chichester, New York, 2011). pp. 511–549.
- [10] M. Quack, J. Stohner and M.A. Suhm, *J. Mol. Struct.* **294**, 33–36 (1993). doi: [10.1016/0022-2860\(93\)80308-I](https://doi.org/10.1016/0022-2860(93)80308-I)
- [11] M. Quack, J. Stohner and M.A. Suhm, *J. Mol. Struct.* **599**, 381–425 (2001). doi: [10.1016/S0022-2860\(01\)00825-0](https://doi.org/10.1016/S0022-2860(01)00825-0).
- [12] W. Klopper, M. Quack and M.A. Suhm, *Mol. Phys.* **94**, 105–119 (1998).
- [13] D. Luckhaus, M. Quack, U. Schmitt and M.A. Suhm, *Ber. Bunsenges. Phys. Chem.* **99**, 457–468 (1995).
- [14] M. Quack, U. Schmitt and M.A. Suhm, *Chem. Phys. Lett.* **269**, 29–30 (1997).
- [15] M. Eigen, *Angew. Chem.* **75**, 489–508 (1963). doi: [10.1002/ange.19630751202](https://doi.org/10.1002/ange.19630751202)
- [16] P. Schuster, *Topics in Current Chemistry, Vol. 120, Hydrogen Bonds* (Springer, Berlin, 1984).
- [17] N. Sheppard, Infrared Spectroscopy and Hydrogen Bonding — Band-widths and Frequency Shifts, in *Hydrogen Bonding*, edited by D. Hadzi (Pergamon Press, London, 1959), pp. 85–106.
- [18] C.B. Aakeröy and K.R. Seddon, *Chem. Soc. Rev.* **22**, 397–407 (1993). doi: [10.1039/CS9932200397](https://doi.org/10.1039/CS9932200397)
- [19] S. Scheiner, *Hydrogen Bonding* (Oxford University Press, New York, 1997).
- [20] G.R. Desiraju and T. Steiner, *The Weak Hydrogen Bond* (Oxford University Press, Oxford, 1999).

- [21] M. Hippler, *Phys. Chem. Chem. Phys.* **4**, 1457–1463 (2002). doi: [10.1039/b110358j](https://doi.org/10.1039/b110358j)
- [22] M. Quack, Symmetry and Evolution: Molecules in Motion Between Less Than Yoctoseconds and More Than Days, *Bunsen-Magazin*. **24**, 238–246 (2022). <https://bunsen.de/bmo/symmetry-and-evolution-molecules-in-motion>.
- [23] W. Klopper, M. Quack and M.A. Suhm, *Chem. Phys. Lett.* **261**, 35–44 (1996).
- [24] R.E. Miller, *Acc. Chem. Res.* **23**, 10–16 (1990). doi: [10.1021/ar00169a003](https://doi.org/10.1021/ar00169a003)
- [25] E.J. Bohac, M.D. Marshall and R.E. Miller, *J. Chem. Phys.* **96**, 6681–6695 (1992). doi: [10.1063/1.462578](https://doi.org/10.1063/1.462578)
- [26] K.v. Puttkamer and M. Quack, *Mol. Phys.* **62**, 1047–1064 (1987).
- [27] K.v. Puttkamer, M. Quack and M.A. Suhm, *Infrared Phys.* **29**, 535–539 (1989).
- [28] M. Quack and M.A. Suhm, *Chem. Phys. Lett.* **183**, 187–194 (1991).
- [29] W. Klopper, M. Quack and M.A. Suhm, *J. Chem. Phys.* **108**, 10096–10115 (1998).
- [30] J. Huang, D. Yang, Y. Zhou and D. Xie, *J. Chem. Phys.* **150**, 154302 (2019). doi: [10.1063/1.5090225](https://doi.org/10.1063/1.5090225)
- [31] R.I. Ovsyannikov, V.Y. Makhnev, N.F. Zobov, J. Koput, J. Tennyson and O.L. Polyansky, *J. Chem. Phys.* **156**, 164305 (2022). doi: [10.1063/5.0083563](https://doi.org/10.1063/5.0083563)
- [32] L.A. Curtiss and J.A. Pople, *J. Mol. Spectrosc.* **48**, 413–426 (1973). doi: [10.1016/0022-2852\(73\)90106-9](https://doi.org/10.1016/0022-2852(73)90106-9)
- [33] D.R. Yarkony, S.V. O’Neil, H.F. Schaefer III, C.P. Baskin and C.F. Bender, *J. Chem. Phys.* **60**, 855–865 (1974). doi: [10.1063/1.1681161](https://doi.org/10.1063/1.1681161)
- [34] H. Lischka, *Chem. Phys. Lett.* **66**, 108–110 (1979).
- [35] J. Gaw, Y. Yamaguchi, M.A. Vincent and H.F. Schaefer III, *J. Am. Chem. Soc.* **106**, 3133–3138 (1984). doi: [10.1021/ja00323a011](https://doi.org/10.1021/ja00323a011)
- [36] M. Kofranek, H. Lischka and A. Karpfen, *Chem. Phys.* **121**, 137–153 (1988). doi: [10.1016/0301-0104\(88\)87012-5](https://doi.org/10.1016/0301-0104(88)87012-5)
- [37] M. Quack and M.A. Suhm, *Mol. Phys.* **69**, 791–801 (1990). doi: [10.1080/00268979000100601](https://doi.org/10.1080/00268979000100601)
- [38] D.H. Zhang, Q. Wu and J.Z.H. Zhang, *J. Chem. Phys.* **102**, 124–132 (1995). doi: [10.1063/1.469382](https://doi.org/10.1063/1.469382)
- [39] D.H. Zhang, Q. Wu, J.Z.H. Zhang, M. v Dirke and Z. Bačić, *J. Chem. Phys.* **102**, 2315–2325 (1995). doi: [10.1063/1.468719](https://doi.org/10.1063/1.468719)
- [40] C.L. Collins, K. Morihashi, Y. Yamaguchi and H.F. Schaefer III, *J. Chem. Phys.* **103**, 6051–6056 (1995). doi: [10.1063/1.470433](https://doi.org/10.1063/1.470433)
- [41] K.A. Peterson and T.H. Dunning, *J. Chem. Phys.* **102**, 2032–2041 (1995). doi: [10.1063/1.468725](https://doi.org/10.1063/1.468725)
- [42] M. Hippler, L. Oeltjen and M. Quack, *J. Phys. Chem. A.* **111**, 12659–12668 (2007). doi: [10.1021/jp076894s](https://doi.org/10.1021/jp076894s)
- [43] K.v. Puttkamer and M. Quack, *Chem. Phys.* **139**, 31–53 (1989).
- [44] S. Albert, K. Keppler Albert and M. Quack, High Resolution Fourier Transform Infrared Spectroscopy, Chapter 26, in *Handbook of High Resolution Spectroscopy*, Vol. 2, M. Quack, F. Merkt (Eds) (Wiley, Chichester, New York, 2011), pp. 965–1019.
- [45] G. Guelachvili and K.N. Rao, *Handbook of Infrared Standards* (Academic Press, Orlando, FL, 1986).
- [46] R. Paso and V.-M. Horneman, *J. Opt. Soc. Am. B.* **12**, 1813–1838 (1995).
- [47] K.v. Puttkamer, M. Quack and M.A. Suhm, *Mol. Phys.* **65**, 1025–1045 (1988). doi: [10.1080/00268978800101581](https://doi.org/10.1080/00268978800101581)
- [48] S. Albert, K. Keppler Albert, H. Hollenstein, C. Manca Tanner and M. Quack, Fundamentals of Rotation-Vibration Spectra, Chapter 3, in *Handbook of High-Resolution Spectroscopy*, Vol. 1, edited by M. Quack, F. Merkt (Wiley, Chichester, New York, 2011). pp. 117–173.
- [49] T.R. Dyke, B.J. Howard and W. Klemperer, *J. Chem. Phys.* **56**, 2442–2454 (1972). doi: [10.1063/1.1677553](https://doi.org/10.1063/1.1677553)
- [50] J.T. Hougen and N. Ohashi, *J. Mol. Spectrosc.* **109**, 134–165 (1985).
- [51] M. Quack, *Mol. Phys.* **34**, 477–504 (1977).
- [52] M. Quack, Fundamental Symmetries and Symmetry Violations from High Resolution Spectroscopy, Chapter 18, in *Handbook of High-Resolution Spectroscopy*, Vol. 1, edited by M. Quack, F. Merkt (Wiley, Chichester, New York, 2011). pp. 659–722.
- [53] M. Quack and M.A. Suhm, *Chem. Phys. Lett.* **171**, 517–524 (1990).
- [54] C.M.A. Brett, J.G. Frey, R. Hinde, Y. Kuroda, R. Marquardt, F. Pavese, M. Quack, J. Stohner and A.J. Thor, *Quantities, Units and Symbols in Physical Chemistry, Abridged Version*, 4th edition (IUPAC and Royal Society of Chemistry, Cambridge and London, 2023).
- [55] E.R. Cohen, T. Cvitaš, J.G. Frey, B. Holmström, K. Kuchitsu, R. Marquardt, I. Mills, F. Pavese, M. Quack, J. Stohner, H.L. Strauss, M. Takami and A.J. Thor, *Quantities, Units and Symbols in Physical Chemistry*, 3rd ed. (IUPAC and Royal Society of Chemistry, Cambridge and London, 2007 and 2011).
- [56] D. Luckhaus, R. Meyer, M. Quack and M.A. Suhm, unpublished results.
- [57] Z. Bačić, Y. Qiu, J.Z.H. Zhang, H.B. Müller and M. Quack, unpublished results.
- [58] J. Blumberger, L. Oeltjen, M. Quack, Z. Bačić, Y. Qiu and J.Z.H. Zhang, *Faraday Disc.* **118**, 431 (2001), and in preparation.
- [59] Y. He, H.B. Müller, M. Quack and M.A. Suhm, *Z. Physik. Chem.* **221**, 1581–1645 (2007).
- [60] X.T. Wu, E.F. Hayes and A.B. McCoy, *J. Chem. Phys.* **110**, 2365–2375 (1999). doi: [10.1063/1.478235](https://doi.org/10.1063/1.478235)
- [61] D.T. Anderson, S. Davis and D.J. Nesbitt, *J. Chem. Phys.* **105**, 4488–4503 (1996).
- [62] G. Herzberg, *Molecular Spectra and Molecular Structure, Volume II, Infrared and Raman Spectra of Polyatomic Molecules* (Van Nostrand, New York, 1945).
- [63] A.S. Pine, W.J. Lafferty and B.J. Howard, *J. Chem. Phys.* **81**, 2939–2950 (1984).
- [64] B. Fehrensens, D. Luckhaus and M. Quack, *Chem. Phys. Lett.* **300**, 312–320 (1999).
- [65] B. Fehrensens, D. Luckhaus and M. Quack, *Chem. Phys.* **338**, 90–105 (2007).
- [66] B. Fehrensens, M. Hippler and M. Quack, *Chem. Phys. Lett.* **298**, 320–328 (1998).
- [67] C. Fabri, R. Marquardt, A.G. Császár and M. Quack, *J. Chem. Phys.* **150**, 014102 (2019). doi: [10.1063/1.5063470](https://doi.org/10.1063/1.5063470)
- [68] C. Maerker, P. v. R. Schleyer, K.R. Liedl, T.K. Ha, M. Quack and M.A. Suhm, *J. Comp. Chem.* **18**, 1695–1719 (1997).
- [69] J. Rezac and P. Hobza, *J. Chem. Theor. Comput.* **10**, 3066–3073 (2014).
- [70] K.v. Puttkamer and M. Quack, *Chimia.* **39**, 358–360 (1985).

- [71] C. Manca, M. Quack and M. Willeke, *Chimia*. **62**, 235–239 (2008).
- [72] W.C. Necochea and D.G. Truhlar, *Chem. Phys. Lett.* **248**, 182–188 (1996).
- [73] M. Quack and M.A. Suhm, *Chem. Phys. Lett.* **234**, 71–76 (1995).
- [74] Z. Bačić and Y. Qiu Vibration-Rotation-Tunneling Dynamics of (HF)₂ and (HCl)₂ from Full Dimensional Quantum Bound State Calculations, in *Advances in Molecular Vibrations and Collision Dynamics*, edited by J.M. Bowman, Z. Bacic (Jai Press, Stamford, CT, 1998), Vol. III, pp. 183–204.
- [75] Y.L. Volobuev and D.G. Truhlar, *Comp. Phys. Commun.* **128**, 516–526 (2000).
- [76] Y. Volobuev, W.C. Necochea and D.G. Truhlar, *Chem. Phys. Lett.* **330**, 471–474 (2000). doi: [10.1016/S0009-2614\(00\)01041-1](https://doi.org/10.1016/S0009-2614(00)01041-1)
- [77] M. Mladenović and M. Lewerenz, *Chem. Phys. Lett.* **321**, 135–141 (2000).
- [78] D.H. Zhang and J.Z.H. Zhang, *J. Chem. Phys.* **98**, 5978–5981 (1993).
- [79] M. von Dirke, Z. Bačić, D.H. Zhang and J.Z.H. Zhang, *J. Chem. Phys.* **102**, 4382–4389 (1995).
- [80] Q. Wu, D.H. Zhang and J.Z.H. Zhang, *J. Chem. Phys.* **103**, 2548–2554 (1995).
- [81] P.M. Felker and Z. Bačić, *J. Chem. Phys.* **151**, 024305 (2019). doi: [10.1063/1.5111131](https://doi.org/10.1063/1.5111131)
- [82] P.M. Felker and Z. Bačić, *Phys. Chem. Chem. Phys.* **24**, 24655–24676 (2022). doi: [10.1039/d2cp04005k](https://doi.org/10.1039/d2cp04005k)
- [83] P.M. Felker and Z. Bačić, *J. Chem. Phys.* **158**, 234109 (2023). doi: [10.1063/5.0156976](https://doi.org/10.1063/5.0156976)
- [84] P.E.S. Wormer and A. van der Avoird, *Chem. Rev.* **100**, 4109–4144 (2000).
- [85] G.W.M. Vissers, G.C. Groenenboom and A. van der Avoird, *J. Chem. Phys.* **119**, 277–285 (2003); **119**, 286–292 (2003).
- [86] M.T. Cvitaš and J.O. Richardson, Quantum Dynamics in Water Clusters, Chapter 9, in *Molecular Spectroscopy and Quantum Dynamics*, edited by R. Marquardt, M. Quack (Elsevier, Amsterdam, 2021). pp. 301–326.
- [87] C. Leforestier, L.B. Braly, K. Liu, M.J. Elrod and R.J. Saykally, *J. Chem. Phys.* **106**, 8527–8544 (1997).
- [88] F.N. Keutsch, N. Goldman, H.A. Harker, C. Leforestier and R.J. Saykally, *Mol. Phys.* **101**, 3477–3492 (2003).
- [89] V. Babin, C. Leforestier and F. Paesani, *J. Chem. Theory Comput.* **9**, 5395–5403 (2013). doi: [10.1021/ct400863t](https://doi.org/10.1021/ct400863t)
- [90] X.G. Wang and T. Carrington, *J. Chem. Phys.* **148**, 074108 (2018). doi: [10.1063/1.5020426](https://doi.org/10.1063/1.5020426)
- [91] G.S. Tschumper, M.L. Leininger, B.C. Hoffman, E.F. Valeev, H.F. Schaefer III and M. Quack, *J. Chem. Phys.* **116**, 690–701 (2002). doi: [10.1063/1.1408302](https://doi.org/10.1063/1.1408302)
- [92] A.E. Barton and B.J. Howard, *Faraday Disc. Chem. Soc.* **73**, 45–62 (1982). doi: [10.1039/DC9827300045](https://doi.org/10.1039/DC9827300045)
- [93] B.L. Feringa, *Angew. Chem. Int. Ed.* **56**, 11060–11078 (2017). doi: [10.1002/anie.201702979](https://doi.org/10.1002/anie.201702979)
- [94] C.L.F. van Beek and B.L. Feringa, *J. Am. Chem. Soc.* **146**, 5634–5642 (2024). doi: [10.1021/jacs.3c14430](https://doi.org/10.1021/jacs.3c14430)
- [95] L. Pauling, *The Nature of the Chemical Bond*, 3rd ed. (Cornell University Press, Ithaca, New York, 1960).
- [96] S. Shaik, D. Danovich and R.N. Zare, *J. Am. Chem. Soc.* **145**, 20132–20140 (2023). doi: [10.1021/jacs.3c08196](https://doi.org/10.1021/jacs.3c08196)
- [97] G. Frenking and S. Shaik, *The Chemical Bond: Fundamental Aspects of Chemical Bonding* (Wiley VCH, Weinheim, 2014). doi: [10.1002/9783527664696](https://doi.org/10.1002/9783527664696)